ADVANCED FUNCTIONAL MATERIALS
www.afm-journal.de

Highly Conductive Ordered Mesoporous Carbon Based Electrodes Decorated by 3D Graphene and 1D Silver Nanowire for Flexible Supercapacitor

*Jian Zhi, Wei Zhao, Xiangye Liu, Angran Chen, Zhanqiang Liu, and Fuqiang Huang**

Ordered mesoporous carbon (OMC) is considered one of the most promising materials for electric double layer capacitors (EDLC) given its low-cost, high specific surface area, and easily accessed ordered pore channels. However, pristine OMC electrode suffers from poor electrical conductivity and mechanical flexibility, whose specific capacitance and cycling stability is unsatisfactory in flexible devices. In this work, OMC is coated on the surface of highly conductive three-dimensional graphene foam, serving as both charge collector and flexible substrate. Upon further decoration with silver nanowires (Ag NWs), the novel architecture of Ag NWs/3D-graphene foam/OMC (Ag-GF-OMC) exhibits exceptional electrical conductivity (up to 762 S cm^{-1}) and mechanical robustness. The Ag-GF-OMC electrodes in flexible supercapacitors reach a specific capacitance as high as 213 F g^{-1}, a value five-fold higher than that of the pristine OMC electrode. Moreover, these flexible electrodes also exhibit excellent long-term stability with >90% capacitance retention over 10 000 cycles, as well as high energy and power density (4.5 Wh kg^{-1} and 5040 W kg^{-1}, respectively). This study provides a new procedure to enhance the device performance of OMC based supercapacitors, which is a promising candidate for the application of flexible energy storage devices.

1. Introduction

Lightweight, flexible, and highly efficient energy storage devices are becoming increasingly pervasive in our daily lives.[1–3] Supercapacitors are widely recognized as an important class of energy storage devices due to the high power capability, moderate energy density, good operational safety, and long cycling stability.[4,5] Currently, much effort has been dedicated to develop flexible electrodes for supercapacitors, mainly using free-standing carbon nanotube films or exfoliated graphene nanosheets (GNS).[6,7] However, in most cases, such high-cost carbon materials are assembled into macroscopic paper-like structures that reduce the accessible surface area for ion adsorption/desorption. This usually results in irreversible agglomeration and restacking of the individual backbones,[8] and leads to low specific capacitance and poor cycling life.

Ordered mesoporous carbon (OMC) is one of the most promising materials for electric double layer capacitors (EDLC) given its low-cost, high specific surface area, and easily accessed ordered pore channels.[9–11] Owing to the regular network of interconnected pore channels in the mesopore size, which can facilitate ion transport and shorten diffusion pathways, the OMC exhibits more excellent rate capability than other carbon based materials.[12,13] However, the specific capacitance of OMC was unsatisfactory because of the relatively low electrical conductivity.[14–16] In order to improve the capacitive performance, graphene-based materials can be introduced into OMC matrix.[17,18] Unfortunately, the composites made from graphene oxide have high electrical resistance coming not only from the intrinsic nano species, but also from grain boundaries. As a result, the development of highly conductive OMC electrodes with excellent mechanical properties is desirable in the field of flexible energy storage devices. More recently, we and the other groups produced a promising freestanding 3D graphene foam structure by chemical vapor deposition (CVD) with nickel foams or Al_2O_3 ceramics as 3D templates.[19–22] The resultant 3D graphene foam displayed excellent electrical conductivity due to the absence of defects and intersheet junction contact resistance. After further coating with silver nanowires (Ag NWs), the obtained Ag NWs/graphene composite exhibited extremely high electrical conductivity (up to 3189 S cm^{-1}).[23] In addition, this 3D structure is bendable and can be directly employed as flexible substrate for functional metal or metal oxides decoration.[8]

In this work, we have developed OMC based highly conductive and flexible electrodes for supercapacitor, employing 3D graphene foam as flexible and conductive scaffold and Ag NWs as conductive reinforcing agent. The obtained Ag NWs/3D-graphene foam/OMC (Ag-GF-OMC) electrodes combine the

Dr. J. Zhi, Dr. W. Zhao, Dr. A. Chen, Dr. Z. Liu, Prof. F. Huang
CAS Key Laboratory of Materials for Energy Conversion
Shanghai Institute of Ceramics
Chinese Academy of Sciences
Shanghai 200050, P. R. China
E-mail: huangfq@mail.sic.ac.cn
Dr. X. Liu, Prof. F. Huang
Beijing National Laboratory for Molecular Sciences
and State Key Laboratory of Rare Earth Materials Chemistry
and Applications, College of Chemistry and
Molecular Engineering, Peking University
Beijing, 100871, P. R. China

DOI: 10.1002/adfm.201303082

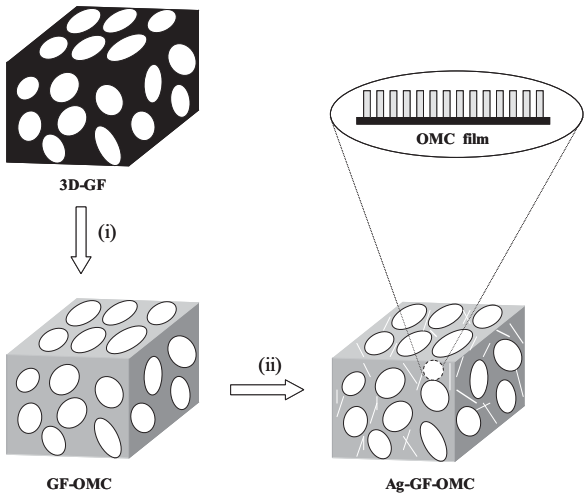

Figure 1. Fabrication of highly conductive OMC based electrode: i) OMC thin film assembly on 3D-graphene foam through dipping and EISA process; ii) Ag NWs coating on GF-OMC network.

advantages of 3D graphene foam and Ag NWs and overcome the poor electrical conductivity and rigidity of pristine OMC, benefitting the practical application of flexible EDLCs. The ultra high electrical conductivity of Ag-GF-OMC (up to 741 S cm^{-1}) allows effective ion and electron transport on the OMC channels and an impressive specific capacitance up to 213 F g^{-1} is achieved, which is much higher than that of the pristine OMC (39 F g^{-1}). Furthermore, the Ag-GF-OMC electrodes also show little capacitance degradation when tested under its normal and highly bent conditions and excellent cycling stability with only 9% capacitance decay over 10 000 charge/discharge cycles, which can be attributed to the outstanding electrical conductivity and mechanical robustness of the 3D interconnected network of Ag-GF-OMC.

2. Results and Discussion

The overall synthetic procedure leading to Ag-GF-OMC architecture is illustrated in **Figure 1**. First, the 3D graphene foam with a weight density of 0.70–0.75 mg cm^{-1} was produced by atmospheric pressure chemical vapor deposition (AP-CVD) on Ni foam for 10 min. After the removal of the Ni substrate, the OMC film was coated on the surface of 3D graphene foam through a solvent evaporation induced self-assembly (EISA) process. In the next step, the 3D graphene foam was dipped into an ethanol solution with resol and F127 as carbon precursor and template, respectively. Within this step, the precursor solution is expected to be uniformly adsorbed on the surface of graphene networks due to the good wettability between ethanol and graphene. After carbonization at 350 °C in Ar atmosphere, the OMC coated 3D graphene foam (GF-OMC) was obtained. Finally, the surface of the carbon networks was decorated with Ag NWs, which were prepared according to previous literature.[23]

The morphology of the 3D-graphene foam is investigated by scanning electron microscopy (SEM), as shown in **Figure 2**a. Obviously, after removal of the Ni template, the graphene replicates the 3D network and porous structure of the Ni foam, and macropores with the size varied from 100 to 500 μm are also maintained, without collapsing and cracking. The quality and layer number of the 3D graphene foam is characterized by Raman spectra (Figure S1, Supporting Information). Only G and 2D bands are observed and D bands are absent in all of the graphene samples, suggesting a high quality. The average layer number of garphene is 8, with the electrical conductivity of 1097 S cm^{-1}.[23] After coating with OMC thin film, the FE-SEM image shows that the surface of the GF-OMC is smooth and no cracking is observed in any domain (Figure S2, Supporting Information). Many large mesopores packed with nanoparticles make the carbonaceous surface much coarser, suggesting open and accessible mesopore channels, which should provide open pathways for ion transportation. Figure 2b shows the SEM image of Ag-GF-OMC. It can be seen that after coating OMC and Ag NWs, the 3D interconnected framework with randomly opened macroporous structure is similar to the original 3D graphene. Remarkably, a high-resolution SEM image (inset of Figure 2b) reveals that the graphene-OMC framework still maintains a flat morphology, while randomly crumpled Ag NWs (tens of micrometers in length) are dispersed on the surface of the OMC films, filling the pores and bridging the grain boundary of the wrinkled OMC films. The decorated Ag NWs can not only further strengthen the mechanical property of the carbon networks, but also act as a conductive bridge to provide effective electron-transport channels. The mesostructure of OMC films on 3D-graphene are also examined by transmission electron

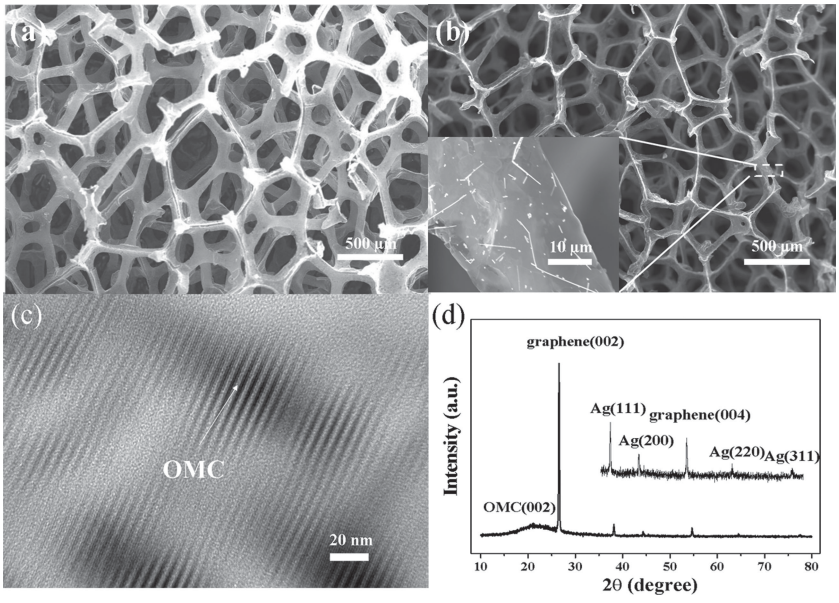

Figure 2. a) SEM of 3D-graphene foam obtained through APCVD method. b) SEM of Ag-GF-OMC, inset illustrating the morphology from the surface of Ag-GF-OMC. c) TEM of OMC film on 3D graphene foam. d) XRD pattern of Ag-GF-OMC.

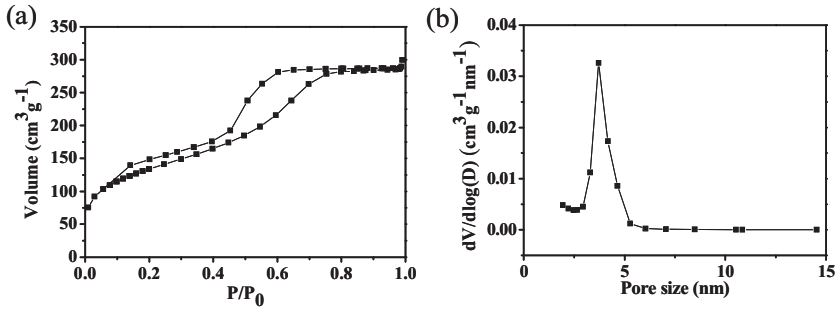

Figure 3. a) Nitrogen sorption isotherms and b) pore size distributions of Ag-GF-OMC.

microscopy (TEM). Figure 2c clearly shows highly ordered hexagonal patterns in large domains on the surface of graphene sheets, indicating the uniform coating of OMC thin films on the 3D graphene framework.

To further characterize the hybrid structure of Ag NWs and OMC film on the surface of 3D graphene foam, the X-ray diffraction (XRD) is performed (Figure 2d). The diffraction peak at 2θ = 38.2°, 44.5°, 64.9°, and 77.9° can be indexed to the (111), (200), (220), and (311) planes of metal Ag, respectively, suggesting the formation of Ag NWs.[23] The 3D graphene shows two diffraction peaks at 2θ = 26.5° and 54.6°, which are attributed to the (002) and (004) planes of graphitic carbon(JCPDS 75–1621), respectively. The sharp peak at 26.5° indicates a high crystallinity and an interlayer space of 0.34 nm of the defect free CVD grown graphene, which is similar to the natural graphite but distinct from the commonly used defective reduced graphene oxide.[24] The wide diffraction peak located at 23° corresponds to (002) planes of carbon materials, further suggesting the existence of OMC thin films.[8] Small-angle X-ray scattering (SAXS) patterns of Ag-GF-OMC are shown in Figure S3, Supporting Information. The four well-resolved scattering peaks can be indexed to 10, 11, 20, and 30 planes of a 2D hexagonal mesostructure (space group *p6m*), indicating a highly ordered mesostructure of the hybrid materials.[25]

The mesoporous feature of Ag-GF-OMC is further confirmed by nitrogen adsorption- desorption measurements (**Figure 3**a). The adsorption-desorption curve exhibits the prominent characteristic of type-IV isotherms with a distinct hysteresis loop in the P/P_0 range of 0.4–1.0, implying the presence of relatively large macropores and mesopores in the frameworks. Moreover, the mesopore size calculated by the BJH method ranges from 3.3 to 4.6 nm with a narrow distribution (Figure 3b), indicating the ideal mesoporous structure of Ag-GF-OMC. Brunauer–Emmett–Teller (BET) analysis reveals a specific surface area of 484 m^2 g^{-1} for Ag-GF-OMC, slightly higher than that of GF-OMC (405 m^2 g^{-1}), and much higher than that of pristine OMC (312 m^2 g^{-1}), owing to its hybrid macro and mesoporous structure.

Electrical measurements of Ag-GF-OMC, GF-OMC, and pristine OMC electrodes with a thickness of about 60 μm were conducted using the four-probe technique with silver electrodes. The electrical conductivity of Ag-GF-OMC as a function of the Ag NWs content is plotted in **Figure 4**a. The conductivity of the Ag-GF-OMC film rapidly increased when Ag NWs were added. It clearly reveals that the Ag NWs have a pronounced effect on the electrical properties of GF-OMC, which is mainly due to the highly conductive Ag NWs bridges on top surface of OMC. The Ag NWs not only fill the pores of OMC films, but also connect the grain boundary between the wrinkled OMC films and uncovered graphene sheets. As a result, a highly conductive network, with the compensation of the conductivity on top of OMC films, is formed after coating Ag NWs. It is noteworthy that the addition of Ag NWs above 4.7 wt% results in a large amount of brittle piles with phase separation and film crushing, which is not suitable for flexible devices.[26] As a result, the optimal content of Ag NWs for our electrode is 4.7 wt%, leading to a conductivity of 764 S cm^{-1}. The GF-OMC electrode also shows outstanding electrical properties with the electrical conductivity up to 413 S cm^{-1}, much higher than that of pristine OMC assembled electrode (13 S cm^{-1}, Figure 4b). In addition, the electrical conductivity of GF-OMC decorated by CNTs was also measured, with the same mass content as Ag-GF-OMC. The electrical conductivity comparison of GF-OMC, Ag-GF-OMC and CNT-GF-OMC was shown in Figure S4, Supporting Information. Compared with Ag-GF-OMC, CNT-GF-OMC exhibits limited enhancement of electrical conductivity over GF-OMC, and the value is 501 S cm^{-1}. It is probably due to the aggregation of CNTs particles on the surface of GF-OMC, as can be seen in the SEM image of CNT-GF-OMC hybrids (Figure S5, Supporting Information).

A flexible supercapacitor with a sandwich configuration was designed, using Ag-GF-OMC composite as symmetric electrodes (**Figure 5**a). Such flexible composites can be directly used as supercapacitor electrodes without adding any binder, which simplifies the assembly in practical applications. The constructed supercapacitors in the flat and bending states are shown in Figure 5b,c. Two pieces of flexible electrode with the same area were separated by filter paper, which was soaked in 6M KOH aqueous electrolyte, followed by encapsulated two pieces of flexible PET. Due to the high electrical conductivity of Ag-GF-OMC, an extra current collector was avoided.

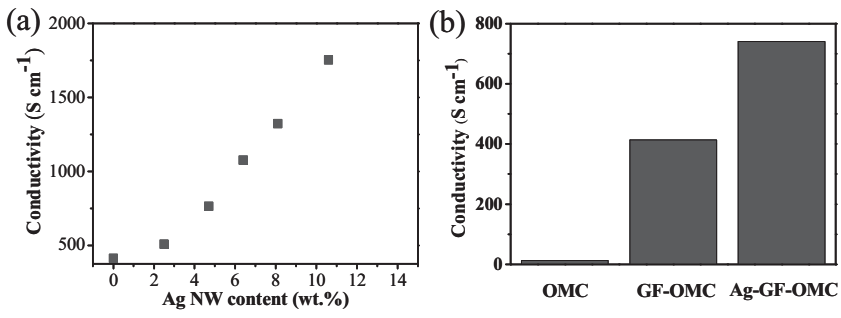

Figure 4. a) Electrical conductivities of Ag-GF-OMC as a function of the Ag NW content. b) Comparison of the electrical conductivities of OMC, GF-OMC, and Ag-GF-OMC.

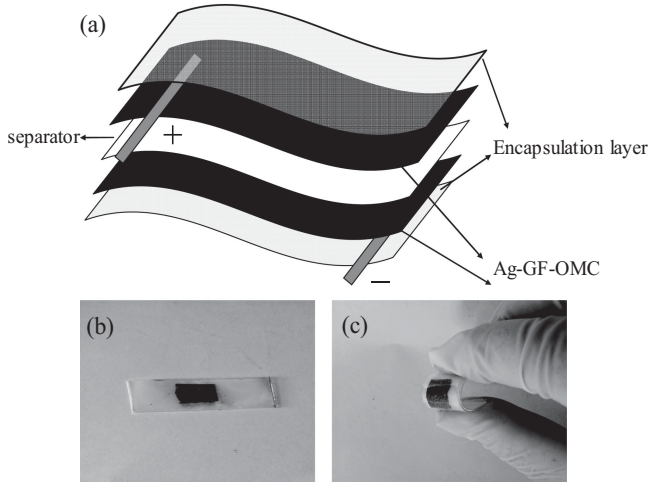

Figure 5. a) Schematic illustration of a flexible supercapacitor using Ag-GF-OMC as electrodes. b,c) Photos of the fabricated flexible supercapacitor in the flat and bending states.

The electrochemical performance of the newly developed flexible Ag-GF-OMC based supercapacitor was measured by using cyclic voltammetry (CV) and galvanostatic curves in 6 M KOH **Figure 6**a,b aqueous solution. As can be seen in Figure 6a, the device exhibited a nearly rectangular CV shape over a wide range of scan rates (0.03–0.1 V s^{-1}), showing a great capacitive behavior. Even at a high scan rate of 0.1 V s^{-1}, the CV curves also retain rectangular shapes with little distortion, indicating low equivalent series resistance (ESR) and fast diffusion of ions from electrolyte into the composite.[27] From Figure 6b, the linear voltage versus time profiles, the symmetrical charge/discharge characteristics, and a quick *I–V* response represent good capacitive characteristics of our supercapacitor. For comparison with Ag-GF-OMC, the capacitive performances of GF-OMC and pristine OMC based devices were also measured, and the curves of specific capacitance versus varied scan rates are shown in Figure 6c. As expected, the highest specific capacitance is observed for Ag-GF-OMC electrodes. The value can reach as high as 213 F g^{-1}, which is higher than that of GF-OMC (139 F g^{-1}) and pristine OMC (36 F g^{-1}). These parallel experiments strongly suggest the critical importance of integrating highly conductive 3D-graphene foams and Ag-NWs to improve the electrochemical performance of pristine OMC.

Electrochemical impedance spectroscopy (EIS) was used to compare the ion-transport behavior and electrical resistance of the Ag-GF-OMC, GF-OMC, and OMC electrodes, as shown in Figure 6d. In the low-frequency region, all the electrodes exhibit a straight and nearly vertical line, characteristic of capacitive behavior. In the high-frequency region (inset of Figure 6d), the real axis intercept is the equivalent series resistance (ESR), and the width of semicircle plotted is indicative of the charge-transfer resistance in the electrode materials.[28] The ESR values of Ag-GF-OMC, GF-OMC, and OMC are 0.7, 1.2, 11.2 Ω, respectively. Moreover, the semicircle observed in the high frequency range corresponded to the charge transfer resistance caused by faradic reactions.[29] The obtained charge transfer resistances of the three materials were 0.89, 1.73, and 7.90 Ω, respectively. The much lower internal and charge transfer resistances observed for Ag-GF-OMC than the other two materials indicate the presence of increased diffusion and migration pathways for electrolyte ions during charge/ discharge processes due to the conductive 3D-graphene and Ag-NWs. Thereby, a synergistic effect of the multicomponent structures is validated: i) The conductive graphene foams within 3D frameworks can serve as multidimensional pathways to facilitate the transport of electrons in the bulk electrode. ii) The Ag-NWs on the surface of OMC film can further enhance ion transport though the OMC channels. iii) The interconnected macro and mesopores frameworks are favorable for buffering ions to shorten the diffusion distances from the external electrolyte to the interior surfaces. As a result, the specific capacitance of such flexible Ag-GF-OMC electrode is comparable to, or even higher than those of OMC based EDLC materials reported recently,[30–36] as shown in **Table 1**. Considering the cell remarks of these electrodes, our devices exhibit more application potential in the field of flexible supercapacitors.

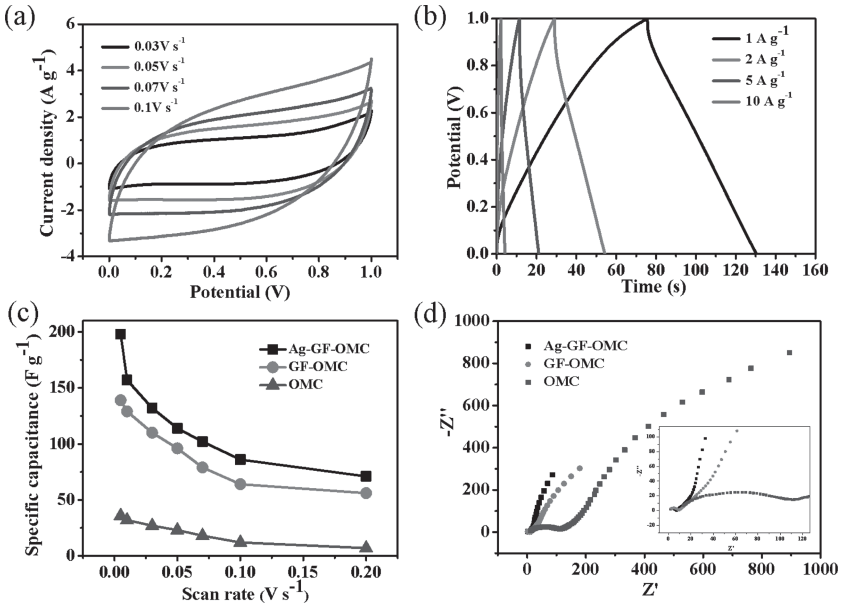

Figure 6. a) CVs of Ag-GF-OMC flexible supercapacitor at scan rates of 0.03, 0.05, 0.07, and 0.1 V s^{-1}. b) Galvanostatic charging/discharging curves of the flexible supercapacitor device at different current densities. c) Specific capacitance of Ag-GF-OMC, GF-OMC, and OMC flexible supercapacitors as a function of scan rates. d) Nyquist plots for Ag-GF-OMC, GF-OMC, and OMC supercapacitors. Inset of (d): an enlarged scale at high frequency.

The electrochemical performance of the flexible Ag-GF-OMC based supercapacitor was also measured in 1 M H_2SO_4 aqueous solution. The nearly rectangular CV shape over a wide range of scan rates (0.03–0.1 V s^{-1}, Figure S6a, Supporting Information) shows a great EDLC behavior of the device in acid electrolyte. The maximum specific capacitance(134 F g^{-1}) was obtained in

Table 1. Comparison of the specific capacitance between the Ag-GF-OMC electrode and several reported OMC-based electrodes

Material	Capacitance [F g^{-1}]	Cell remarks	Refs.
CA-OMC	165	Three electrodes	[30]
OMCs	90	Three electrodes	[31]
OMCs	188	Three electrodes	[32]
OMCs	148	Three electrodes	[33]
OMCs	180	Three electrodes	[34]
OMCs	173	Two electrodes	[35]
OMCs	172	Free standing, three electrodes	[36]
Ag-GF-OMC	213	Flexible, two electrodes	Our work

the scan rate of 0.005 V s^{-1}(Figure S6b, Supporting Information), which is comparable with the specific capacitance of previously reported carbon materials in acid electrolyte.[37,38]

In order to demonstrate the flexibility of our device, we measured CV curves of Ag-GF-OMC at the scan rate of 0.05 V s^{-1} with a bending angle of 90°. As shown in **Figure 7**a, there is no significant difference between the CV curves with and without bending, suggesting the highly flexible property for the Ag-GF-OMC based symmetrical supercapacitor. This can be attributed to the synergistic effects from the integration of Ag NWs, OMC film and 3D-graphene foams. The cycling performance of the flexible supercapacitors with electrodes of Ag-GF-OMC, GF-OMC and OMC for cycling test with a bending angle of 90°, were also performed (Figure 7b). The resulting specific capacitance of Ag-GF-OMC retained 92% of its initial value even after 200 bending actions, indicating its excellent mechanical and flexible properties. The GF-OMC exhibited the similar behavior attributing to the flexibility of 3D-graphene foam, while OMC showed the lowest capacitance retention after 200 cycles, indicating the breaking of the electrode after bending. Moreover, Ag-GF-OMC exhibits an acceptable cycling stability performance over the range 0 to 1 V at a scan rate of 0.1 V s^{-1} (Figure 7c). The specific capacitance value remained at 91% of the initial value after 10 000 consecutive cycles, demonstrating the excellent electrochemical stability of the present electrode material. To further evaluate the performance of the flexible devices, we have plotted the Ragone plot to compare our devices with a few typical examples reported in the literature to date (Figure 7d). The flexible supercapacitor exhibits an energy density of 4.5 Wh kg^{-1} at a power density of 250 W kg^{-1} for a 1 V window voltage. It also preserves 16% of its energy density as the power density increases up to 5040 W kg^{-1}. These values are superior to the similar carbon based symmetrical EDLC systems reported recently, such as RGO//RGO,[39] SWCNT//SWCNT,[37] graphene-cellulose//graphene-cellulose,[38] AC//AC,[35] and graphene//graphene.[40]

3. Conclusion

In summary, we have reported a novel OMC based highly conductive and flexible supercapacitor to achieve a high specific capacitance (213 F g^{-1}), excellent cycling stability (9% capacitance decay over 10 000 CV circles), high energy and power density (4.5 Wh kg^{-1} and 5040 W kg^{-1}, respectively) and outstanding mechanical flexibility. Such a high performance can be ascribed to the following features: 1) The high conductivity and porous structure of the Ag-GF-OMC serve as a highway for electron transfer and easy access for electrolyte ions to the electrode surfaces. 2) The good contact between the graphene and OMC thin film produced by EISA process ensures low contact resistance and tight adhesion, which can survive large and repeated bending deformations. 3) The high specific surface area and hierarchical structure of the Ag-GF-OMC networks give a large active surface area and full accessibility for the electrolyte charged ions. On the basis of these intriguing features, the high-performance electrochemical behavior of the hybrid OMC electrode renders it a promising candidate for a flexible supercapacitor. Furthermore, the simple and low-cost assembly of this flexible supercapacitor can largely extent the potential applications of OMC based devices, such as energy supply systems for small flying devices, adhesive tape-like supercapacitors, wearable supercapacitors, and so on.

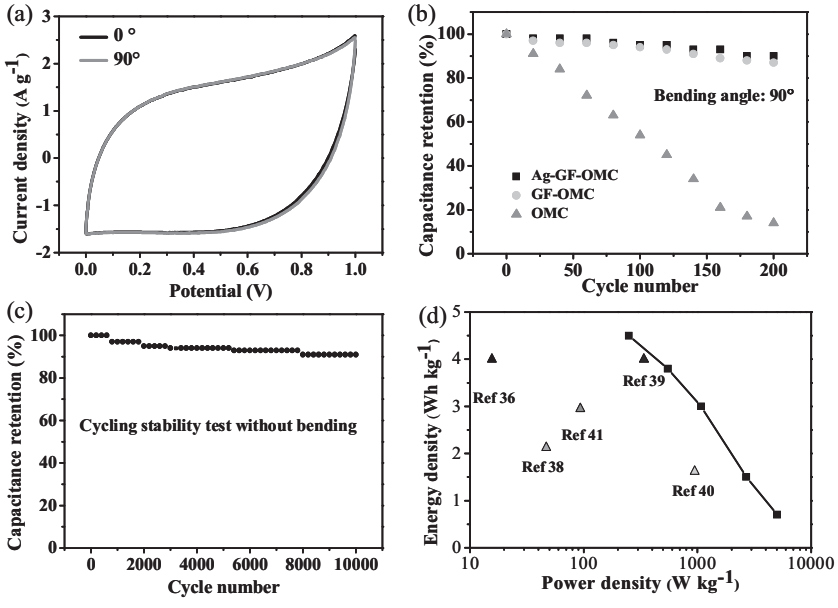

Figure 7. a) Comparison of CV curves at 0.05V s^{-1} for Ag-GF-OMC flexible supercapacitor tested as normal and bent. b) Cycling performance of Ag-GF-OMC, GF-OMC, and OMC flexible supercapacitors for bending cycles with a bending angle of 90° at a scan rate of 0.1 V s^{-1}. c) Cycling life performance of Ag-GF-OMC at a scan rate of 0.1 V s^{-1}. d) Ragone plots of the flexible supercapacitor, compared with the values of similar symmetrical systems.

4. Experimental Section

3D-Graphene Foam Preparation: Ni foams were used to catalyze the graphene growth. Firstly, Ni

foams were immersed in a dilute solution of acetic acid for 30 min to remove the oxide layer on their surface, then washed in isopropanol and acetone for 10 min, respectively, and finally rinsed with deionized water and dried for use. Secondly, the Ni foams were heated to 1000 °C in 40 min under H_2 (200 sccm), then a gas mixture flow of CH_4, H_2, and Ar was introduced to initiate graphene growth for 10–30 min. After growth, the samples were rapidly cooled to 500 °C at a rate of 200 °C min^{-1} under Ar and H_2. The Ni foams covered with graphene were drop-coated with a poly(methyl methacrylate) (PMMA) solution (4% in anisole), and then baked at 100 °C for 2 h. The PMMA/graphene/Ni foam structure was obtained after solidification. Then the samples were put into a 5 M HCl solution for 5 h to completely dissolve the Ni foams to obtain the PMMA/graphene. Finally three-dimensional graphene networks were obtained after removing PMMA in acetone.

GF-OMC Preparation: 0.61 g of phenol was melted at 40–42 °C in a flask and mixed with 0.13 g of 20 wt% sodium hydroxide (NaOH) aqueous solution under stirring. After 10 min, 1.05 g of formalin (37 wt% formaldehyde) was added dropwise below 50 °C. Upon further stirring for 1 h at 70–75 °C, the mixture was cooled to room temperature. The pH was adjusted with 0.6 M HCl solution until it reached a value of 7.0, and water was removed by vacuum evaporation below 50 °C. The final product was dissolved in ethanol. In a typical preparation of the sol of mesoporous carbon precursor, 1.0 g of F127 was dissolved in 20.0 g of ethanol. Then 5.0 g of resol precursors in ethanol solution containing 0.61 g of phenol and 0.39 g of formaldehyde was added. After stirring for 10 min, a homogeneous solution was obtained. The previous fabricated 3D-graphene(1 cm × 1 cm) was then dipped into the sol, and removed immediately. the product was transferred into dishes to evaporate ethanol at room temperature for 5–8 h, followed by heating in an oven at 100 °C for 24 h. Calcination was carried out in a tubular furnace under an Ar atmosphere at 350 °C for 3 h, and the heating rate was 1 °C min^{-1}.

Ag-GF-OMC Preparation: Ag NWs were prepared through previous reported literature.[23] Ag NWs were dispersed in deionized water, and the concentration was about 0.2 mg mL^{-1}. After bath sonication for 5 min, the Ag NWs suspension was dipped on the surface of GF-OMC monolith. The amount of Ag NWs was controlled by adjusting the volume of the Ag NWs suspension. The excess water was evaporated at room temperature, and Ag-GF-OMC (4.7% Ag NWs, w/w) was obtained.

CNT-GF-OMC Preparation: commercial available carbon nanotubes (CNTs, TIMESNANO) were dispersed in ethanol, and the concentration was about 0.2 mg mL^{-1}. After bath sonication for 5 min, the CNTs suspension was dipped on the surface of GF-OMC monolith. The amount of CNTs was controlled by adjusting the volume of the CNTs suspension. The excess ethanol was evaporated at room temperature, and CNT-GF-OMC (4.7% CNTs, w/w) was obtained.

Electrochemical Measurement: The flexible supercapacitor was assembled to measure the device performances. In detail, Ag-GF-OMC (area of 1 cm by 1 cm) with a mass loading of 1 mg cm^{-2} was attached on the PET membrane as both electrodes and current collectors. Two pieces of these sheets were assembled with a 120 μm thick membrane, separated with filter paper and sandwiched in between (Figure 4a). GF-OMC based flexible supercapacitor was assembled according to the similar procedures. For comparison, free standing OMC thin film based supercapacitor, without attaching 3D-graphene foam, was assembled according to the previous literature.[41] Copper wires were embedded and connected to carbon materials with silver paste, which enables a strong electrical contact and a small contact resistance between the copper wires and the active materials. The electrolyte used in all of the measurements was a 6 M KOH or 1 M H_2SO_4 aqueous solution, which was sealed by adhesive tape.

Characterization and Measurement: The morphologies and structures of the graphene papers were investigated by SEM (JEOL JSM-6510 and Hitachi S-4800), XRD (Bruker D8 Advance), HRTEM (JEOL JEM 2100F), and SAXS (Nanostar U). The electrical properties of graphene papers were measured by the Van der Pauw method with an Accent HL5500. N_2 sorption isotherms were measured with a MicromeriticsModel Tristar 3000 analyzer at 77 K. Before the measurements, all samples were degassed at 180 °C under vacuum for at least 6 h. Using the Barrett- Joyner-Halenda (BJH) model, the pore volumes and pore size distributions were derived from the adsorption branches of isotherms. The Brunauer-Emment-Teller (BET) method was utilized to calculate the specific surface areas.

All the electrochemical experiments were carried out using a CHI 660B workstation. The electrochemical impedance spectroscopy measurements were performed over a frequency range from 10^5 to 10^{-2} Hz at an amplitude of 5 mV. The cycle life tests were conducted by CV measurements with a constant scan rate of 0.1 V s^{-1} for 10 000 cycles. The specific capacitance derived from CV curves was calculated according to the following equation: $C_S = 2(\int I\,dV)/vm\Delta V$, where I is the voltammetric current, m is the total mass of one electrode, v is the potential scan rate, and V is the potential in one sweep segment. The specific capacitance derived from galvanostatic discharge curves was calculated based on the following equation: $C_g = 2(I\Delta t)/(m\Delta V)$, where I is the discharge current, Δt is the time for a full discharge, m is the total mass of one electrode, and ΔV represents the potential change after a full discharge. The energy density (E) and power density (P) of one electrode depicted in the Ragone plots were calculated by using the equations $E = (1/8)\ C_g\Delta V^2$ and $P = E/\Delta t$, respectively, where C_g is the specific capacitance derived from galvanostatic discharge curves, ΔV is the potential change after a full discharge, and Δt is the time for a full discharge.

Supporting Information

Supporting Information is available from the Wiley Online Library or from the author.

Acknowledgements

J.Z. and W.Z. contributed equally to this work. Financial support from National 973 Program of China (Grant no. 2009CB939900), Graphene Project of CAS (Grant no. KGZD-EW-303), NSF of China (Grants no. 51125006, 91122034, 51121064, 21101164, 61076062, 51202275) is acknowledged.

Received: September 4, 2013
Revised: October 14, 2013
Published online: November 27, 2013

[1] S. Ju, A. Facchetti, Y. Xuan, J. Liu, F. Ishikawa, P. Ye, C. Zhou, T. J. Marks, D. B. Janes, *Nat. Nanotechnol.* **2007**, *2*, 378.
[2] Q. Cao, H.-s. Kim, N. Pimparkar, J. P. Kulkarni, C. Wang, M. Shim, K. Roy, M. A. Alam, J. A. Rogers, *Nature* **2008**, *454*, 495.
[3] D.-H. Kim, N. Lu, R. Ma, Y.-S. Kim, R.-H. Kim, S. Wang, J. Wu, S. M. Won, H. Tao, A. Islam, K. J. Yu, T.-i. Kim, R. Chowdhury, M. Ying, L. Xu, M. Li, H.-J. Chung, H. Keum, M. McCormick, P. Liu, Y.-W. Zhang, F. G. Omenetto, Y. Huang, T. Coleman, J. A. Rogers, *Science* **2011**, *333*, 838.
[4] P. Simon, Y. Gogotsi, *Nat. Mater.* **2008**, *7*, 845.
[5] T. Brezesinski, J. Wang, S. H. Tolbert, B. Dunn, *Nat. Mater.* **2010**, *9*, 146.
[6] D.-W. Wang, F. Li, J. Zhao, W. Ren, Z.-G. Chen, J. Tan, Z.-S. Wu, I. Gentle, G. Q. Lu, H.-M. Cheng, *ACS Nano* **2009**, *3*, 1745.
[7] Q. Wu, Y. Xu, Z. Yao, A. Liu, G. Shi, *ACS Nano* **2010**, *4*, 1963.
[8] Y. He, W. Chen, X. Li, Z. Zhang, J. Fu, C. Zhao, E. Xie, *ACS Nano* **2012**, *7*, 174.
[9] K. Jurewicz, C. Vix-Guterl, E. Frackowiak, S. Saadallah, M. Reda, J. Parmentier, J. Patarin, F. Béguin, *J. Phys. Chem. Solids* **2004**, *65*, 287.

[10] S. Álvarez, M. C. Blanco-López, A. J. Miranda-Ordieres, A. B. Fuertes, T. A. Centeno, *Carbon* **2005**, *43*, 866.
[11] H.-Q. Li, J.-Y. Luo, X.-F. Zhou, C.-Z. Yu, Y.-Y. Xia, *J. Electrochem. Soc.* **2007**, *154*, A731.
[12] R. Ryoo, S. H. Joo, M. Kruk, M. Jaroniec, *Adv. Mater.* **2001**, *13*, 677.
[13] S. Jun, S. H. Joo, R. Ryoo, M. Kruk, M. Jaroniec, Z. Liu, T. Ohsuna, O. Terasaki, *J. Am. Chem. Soc.* **2000**, *122*, 10712.
[14] L. L. Zhang, R. Zhou, X. S. Zhao, *J. Mater. Chem.* **2010**, *20*, 5983.
[15] M. Inagaki, H. Konno, O. Tanaike, *J. Power Sources* **2010**, *195*, 7880.
[16] P. Liu, Y. Huang, L. Wang, *Mater. Lett.* **2013**, *97*, 173.
[17] M. Li, J. Ding, J. Xue, *J. Mater. Chem. A* **2013**, *1*, 7469.
[18] L. Wang, L. Sun, C. Tian, T. Tan, G. Mu, H. Zhang, H. Fu, *RSC Adv.* **2012**, *2*, 8359.
[19] H. Bi, F. Huang, J. Liang, Y. Tang, X. Lu, X. Xie, M. Jiang, *J. Mater. Chem.* **2011**, *21*, 17366.
[20] Z. Chen, W. Ren, L. Gao, B. Liu, S. Pei, H.-M. Cheng, *Nat. Mater.* **2011**, *10*, 424.
[21] X.-C. Dong, H. Xu, X.-W. Wang, Y.-X. Huang, M. B. Chan-Park, H. Zhang, L.-H. Wang, W. Huang, P. Chen, *ACS Nano* **2012**, *6*, 3206.
[22] M. Zhou, T. Lin, F. Huang, Y. Zhong, Z. Wang, Y. Tang, H. Bi, D. Wan, J. Lin, *Adv. Funct. Mater.* **2013**, *23*, 2263.
[23] J. Chen, H. Bi, S. Sun, Y. Tang, W. Zhao, T. Lin, D. Wan, F. Huang, X. Zhou, X. Xie, M. Jiang, *ACS Appl. Mater. Interfaces* **2013**, *5*, 1408.
[24] S. Park, J. An, J. R. Potts, A. Velamakanni, S. Murali, R. S. Ruoff, *Carbon* **2011**, *49*, 3019.
[25] H. Wei, Y. Lv, L. Han, B. Tu, D. Zhao, *Chem. Mater.* **2011**, *23*, 2353.
[26] K.-Y. Chun, Y. Oh, J. Rho, J.-H. Ahn, Y.-J. Kim, H. R. Choi, S. Baik, *Nat. Nanotechnol.* **2010**, *5*, 853.
[27] S. Bose, T. Kuila, A. K. Mishra, R. Rajasekar, N. H. Kim, J. H. Lee, *J. Mater. Chem.* **2012**, *22*, 767.
[28] K. Wang, P. Zhao, X. Zhou, H. Wu, Z. Wei, *J. Mater. Chem.* **2011**, *21*, 16373.
[29] J. Zhi, S. Deng, Y. Zhang, Y. Wang, A. Hu, *J. Mater. Chem. A* **2013**, *1*, 3171.
[30] D. Wu, X. Chen, S. Lu, Y. Liang, F. Xu, R. Fu, *Microporous Mesoporous Mater.* **2010**, *131*, 261.
[31] L. Wang, Y. Zhou, J. Qiu, *Microporous Mesoporous Mater.* **2013**, *174*, 67.
[32] M. C. Kao, H. Z. Chen, S. L. Young, C. Y. Kung, C. C. Lin, *Thin Solid Films* **2009**, *517*, 5096.
[33] F. Li, N. van der Laak, S.-W. Ting, K.-Y. Chan, *Electrochim. Acta* **2010**, *55*, 2817.
[34] W. Xing, S. Z. Qiao, R. G. Ding, F. Li, G. Q. Lu, Z. F. Yan, H. M. Cheng, *Carbon* **2006**, *44*, 216.
[35] J. Sánchez-González, F. Stoeckli, T. A. Centeno, *J. Electroanal. Chem.* **2011**, *657*, 176.
[36] E. Kang, G. Jeon, J. K. Kim, *Chem. Commun.* **2013**, *49*, 6406.
[37] M. Kaempgen, C. K. Chan, J. Ma, Y. Cui, G. Gruner, *Nano Lett.* **2009**, *9*, 1872.
[38] Z. Weng, Y. Su, D.-W. Wang, F. Li, J. Du, H.-M. Cheng, *Adv. Energy Mater.* **2011**, *1*, 917.
[39] J. Zhang, J. Jiang, H. Li, X. S. Zhao, *Energy Environ. Sci.* **2011**, *4*, 4009.
[40] Z.-S. Wu, W. Ren, D.-W. Wang, F. Li, B. Liu, H.-M. Cheng, *ACS Nano* **2010**, *4*, 5835.
[41] D. Feng, Y. Lv, Z. Wu, Y. Dou, L. Han, Z. Sun, Y. Xia, G. Zheng, D. Zhao, *J. Am. Chem. Soc.* **2011**, *133*, 15148.